ARTICLE

doi:10.1038/nature16442

Acute off-target effects of neural circuit manipulations

Timothy M. Otchy[1,2], Steffen B. E. Wolff[1]*, Juliana Y. Rhee[1]*, Cengiz Pehlevan[3]*, Risa Kawai[1], Alexandre Kempf[1]†, Sharon M. H. Gobes[1]† & Bence P. Ölveczky[1,4]

Rapid and reversible manipulations of neural activity in behaving animals are transforming our understanding of brain function. An important assumption underlying much of this work is that evoked behavioural changes reflect the function of the manipulated circuits. We show that this assumption is problematic because it disregards indirect effects on the independent functions of downstream circuits. Transient inactivations of motor cortex in rats and nucleus interface (Nif) in songbirds severely degraded task-specific movement patterns and courtship songs, respectively, which are learned skills that recover spontaneously after permanent lesions of the same areas. We resolve this discrepancy in songbirds, showing that Nif silencing acutely affects the function of HVC, a downstream song control nucleus. Paralleling song recovery, the off-target effects resolved within days of Nif lesions, a recovery consistent with homeostatic regulation of neural activity in HVC. These results have implications for interpreting transient circuit manipulations and for understanding recovery after brain lesions.

Understanding how the brain generates behaviour is a daunting task often simplified by studying anatomically distinct brain regions in isolation. The underlying assumption is that different parts of the brain are specialized for different functions that can be understood by monitoring and altering activity in local circuits. An increasingly powerful and widely used approach is to transiently silence or otherwise perturb—by optogenetic, pharmacological or other means—neural activity in specific circuits and observe the consequences on behaviour[1,2]. If there is an effect, the conclusion is that the circuit under investigation is causally 'involved' in the behaviour. But what does such a causal link actually tell us?

In a densely interconnected dynamical system like the brain, sudden perturbations to one node (for example, a brain area) could send ripples through the system, compromising the capacity of downstream circuits to perform computations on other inputs or generate patterned activity from internal dynamics[3,4]. Given the reliance on transient circuit manipulations for localizing computations and memory functions to specific neural circuits or brain areas[1,2], the caveats and limitations of these methods should be scrutinized.

If inactivating a brain area interferes with the independent functions of downstream circuits, that is, functions not contingent on information provided by the targeted area, an important next question is whether those functions remain compromised after the silencing is made permanent through lesions. For example, deficits caused by changes in the excitability of downstream neurons could plausibly resolve through homeostatic regulation of neural activity[5–9]. Spontaneous recalibration of neural dynamics, more generally, could help explain why chronic effects of permanent lesions are often far less severe than those induced by transient inactivations[10–12], and why patients with strokes and other brain injuries can overcome some of their initial deficits without rehabilitation[13].

Functional recovery after brain lesions, however, is thought to be driven predominantly by the adoption of new behavioural strategies and the adaptive repurposing of non-lesioned circuits[12,14], processes contingent on renewed experience with affected tasks[15]. Therefore, demonstrating acute off-target effects of inactivations and spontaneous recovery after permanent lesions requires showing that task-specific behaviours sensitive to transient inactivations can recover after lesions without additional task experience. As experience-dependent recovery is difficult to rule out for basic sensory or motor functions that are central to many behaviours and hence naturally 'practiced' after lesions[10,11,1] , our study used behaviours for which such incidental practice can be withheld. We chose learned movement sequences of rats[16] and courtship songs of zebra finches[17] because they are task-specific skills associated with complex, stereotyped and idiosyncratic motor patterns that can be precisely quantified and compared across various manipulations.

To probe the effects of transient manipulations on distinct and independent functions of downstream circuits, we targeted brain areas—motor cortex in rats and the sensorimotor area Nif in songbirds—that are known, based on lesion studies, to be dispensable for storing and executing the skills we study[16,1] . Despite this, transient manipulations severely degraded the learned behaviours in both systems. These discrepancies were consistent with acute disruptions of downstream circuit function. Though we saw similar behavioural effects immediately after permanent lesions, they resolved spontaneously, leading to full recovery of the initially affected behaviours.

Motor cortex inactivation disrupts skill execution

In our motor learning task, rats are rewarded for pressing a lever in a precise temporal sequence (two presses 700 ms apart, Fig. 1a). Animals solve this task by acquiring spatiotemporally precise movement patterns that produce the prescribed lever-press sequence[16]. Though the learned skills are robust to motor cortical lesions[16], motor cortex projects to sub-cortical motor structures whose distinct functions could be sensitive to sudden changes in motor cortical input (Fig. 1b). To probe this, we inactivated primary forelimb motor cortex of rats that had learned the task ($n = 5$ rats) by injecting 100 nl of the $GABA_A$ agonist

[1]Center for Brain Science, Harvard University, Cambridge, Massachusetts 02138, USA. [2]Program in Neuroscience, Harvard University, Cambridge, Massachusetts 02138, USA. [3]Center for Computational Biology, Simons Foundation, New York, New York 10010, USA. [4]Department of Organismic and Evolutionary Biology, Harvard University, Cambridge, Massachusetts 02138, USA.
†Present addresses: Institut de Biologie, Ecole Normale Supérieure, Paris, France (A.K.); Neuroscience Program, Wellesley College, Wellesley, Massachusetts 02481, USA (S.M.H.G.).
*These authors contributed equally to this work.

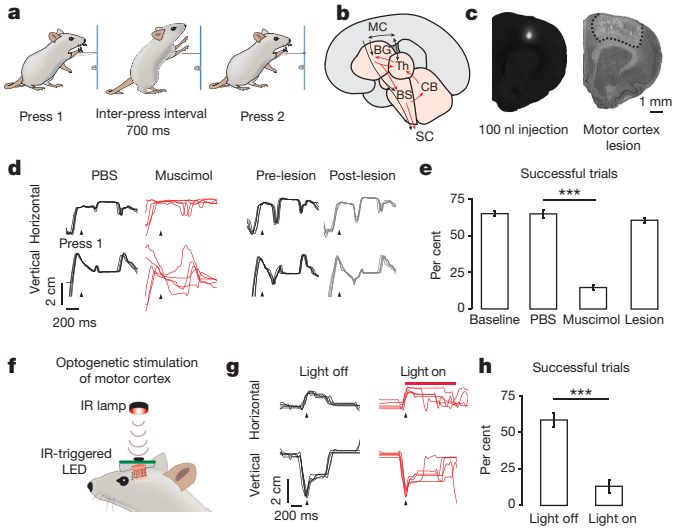

Figure 1 | Motor skills that survive motor cortical lesions are acutely affected by transient manipulations of motor cortex. a, We used a motor skill learning paradigm that trains rats to press a lever twice with a specified inter-press interval (IPI), typically 700 ms. **b**, Schematic of the mammalian motor system. Motor cortex (MC, black) provides input to subcortical circuits (red shaded regions, BG, basal ganglia; CB, cerebellum; BS, brainstem; Th, thalamus; SC, spinal cord). **c**, Coronal sections comparing the spread of a fluorescent marker (fluorescein) matched in concentration and volume to our muscimol injections (left) with motor cortex lesions that leave the learned skills intact[16] (right, dashed lines denote the lesioned area) (Methods). **d**, Left, forepaw trajectories associated with five consecutive trials after PBS and muscimol injections for the rat that received the lowest dose of muscimol (100 nl, 1 mM) (Supplementary Video 1). Right, motor cortex was subsequently lesioned in this rat. Paw trajectories associated with five consecutive trials from the last training session before and the first training session after the lesion. **e**, Fraction of trials with IPIs within 20% of the target ('successful' trials) for different experimental conditions ($n = 5$ rats). Lesion data from ref. 16 shown for comparison (light-grey bar). **f**, Wireless optogenetic stimulation (Methods). **g**, Paw trajectories for five consecutive trials for an example rat with and without optogenetic stimulation of motor cortex. **h**, Same as **e**, but with and without optogenetic stimulation of motor cortex ($n = 5$ rats). Error bars represent standard error of the mean (s.e.m.). $***P < 0.001$. For tests of significance for this and all other figures see Methods.

muscimol (1–25 mM) into the hemisphere contralateral to the dominant paw[19,20] (Methods). Based on previous studies[21] and injections of 100 nl of fluorescein into motor cortex (Fig. 1c), we estimate that the direct effects of our injections were confined to a volume far smaller than our previous lesions[16] (Fig. 1c; Methods).

In contrast to animals tested for the first time 5–10 days after lesions[16], muscimol-injected rats had severe deficits in skill execution with marked drops in performance and disrupted paw kinematics (Fig. 1d, e). These effects were evident even in the rat receiving the lowest concentration of muscimol (1 mM) (rat in Fig. 1d, Supplementary Video 1). We later lesioned motor cortex in this rat, and as previously reported (rat 'Kansas' in ref. 16), saw no effect on skill execution when the rat was tested again 10 days post-lesion (Fig. 1d).

To explore dose-dependence, we injected larger volumes of muscimol in two of the rats (200 nl and 400 nl respectively). We found task performance to be even more affected with lever-interactions restricted to a few single presses with no rewarded trials (Supplementary Video 1).

Optogenetic stimulation of motor cortex

Transient stimulation of neural activity is an alternative method for disrupting ongoing circuit dynamics that is well-suited for interrogating processes associated with precise and reproducible neural dynamics[22]. As with transient inactivations, sudden activation can also plausibly affect the dynamics and function of downstream circuits. To probe the effect of transient motor cortex stimulation on skill execution, we used optogenetics, a widely adopted method for manipulating neurons in temporally specific ways[23].

We expressed the optogenetic activator Chrimson[24] in motor cortex ($n = 5$ rats; Extended Data Fig. 1a, b; Methods), and stimulated the hemisphere contralateral to the dominant paw after animals had reached asymptotic performance on the task (Fig. 1f and Extended Data Fig. 1c). Neither brief (50 ms) nor sustained (1 s) optogenetic stimulation evoked visible motor responses during rest, suggesting that they were sub-threshold for movement initiation. However, both brief and sustained stimulation, triggered on the first lever-press in a trial, interfered with task performance and associated kinematics (Fig. 1g, h, Extended Data Fig. 2 and Supplementary Video 2). Thus, similar to transient inactivations, disrupting normal activity patterns in motor cortex by optogenetic stimulation compromises the animals' capacity to execute skills robust to permanent lesions.

Effects of Nif lesions and inactivations differ

Our results suggested that behavioural effects of transient perturbations may overestimate the steady-state functions of targeted circuits. To examine whether this caveat should be considered more broadly, we similarly probed whether transient inactivations of sensorimotor nucleus Nif in zebra finches affect their courtship songs. Although the song survives Nif lesions[18], Nif sends excitatory projections to HVC, an essential part of the song control circuit believed to generate the temporal pattern for learned vocalizations through intrinsic network dynamics[25] (Fig. 2a and Extended Data Fig. 3a).

We first confirmed the findings of previous lesion studies[18] by injecting 27–36 nl of *N*-methyl-DL-aspartic acid (NMA), an excitotoxin, bilaterally into Nif ($n = 5$ birds) (Fig. 2a and Extended Data Fig. 3b). When Nif lesioned birds resumed singing two days after surgery, their songs were similar to pre-lesion (Fig. 2b, c), consistent with prior studies. Because birds did not sing within the first day of lesions, this result does not preclude short-term effects of Nif silencing[18]. To probe such acute effects, we injected 27 nl of muscimol (50 mM) bilaterally into Nif of awake head-restrained adult birds ($n = 5$ birds; Fig. 2d, e, Extended Data Fig. 4a; Methods).

Birds typically sang within 20 min of the injections, but their songs were severely degraded and reminiscent of subsong (Fig. 2f, g), highly variable and unstructured utterances normally produced by juvenile birds at the start of vocal learning or by adult birds after bilateral HVC lesions[26]. The syllable duration distributions were similar to those reported in HVC-lesioned birds[26] (Fig. 2h), suggesting that Nif inactivation degrades song by indirectly affecting HVC dynamics.

To exclude the possibility that the behavioural effects were caused by diffusion of muscimol into HVC, we injected the same dose 300–500 μm dorsal to Nif but closer to HVC ($n = 5$ birds), as well as smaller volumes (9 nl) into Nif ($n = 2$ birds). The control injections above Nif did not affect song (Fig. 2f, g), whereas the smaller Nif injections evoked effects similar to the larger dose (Extended Data Fig. 4b).

HVC dynamics recover after Nif lesion

Transient circuit manipulations performed in both rats and songbirds revealed strong effects on skill execution not seen after permanent lesions (Figs 1 and 2). The discrepancy could not be explained by experience-dependent relearning in lesioned animals because the skills recovered their idiosyncratic pre-lesion form without any intervening practice (Figs 1d, e and 2b, c)[16]. However, the acute behavioural deficits were consistent with activity manipulations in motor cortex and Nif indirectly affecting the independent functions of downstream circuits. These initially affected circuits, however, seemingly regained their capacity to execute the learned behaviours after permanent lesions[16,18].

Unlike in rats, where the neural circuits underlying the skills we assay have yet to be characterized, the vocal control circuits in zebra finches have been well delineated[27], making it feasible to investigate

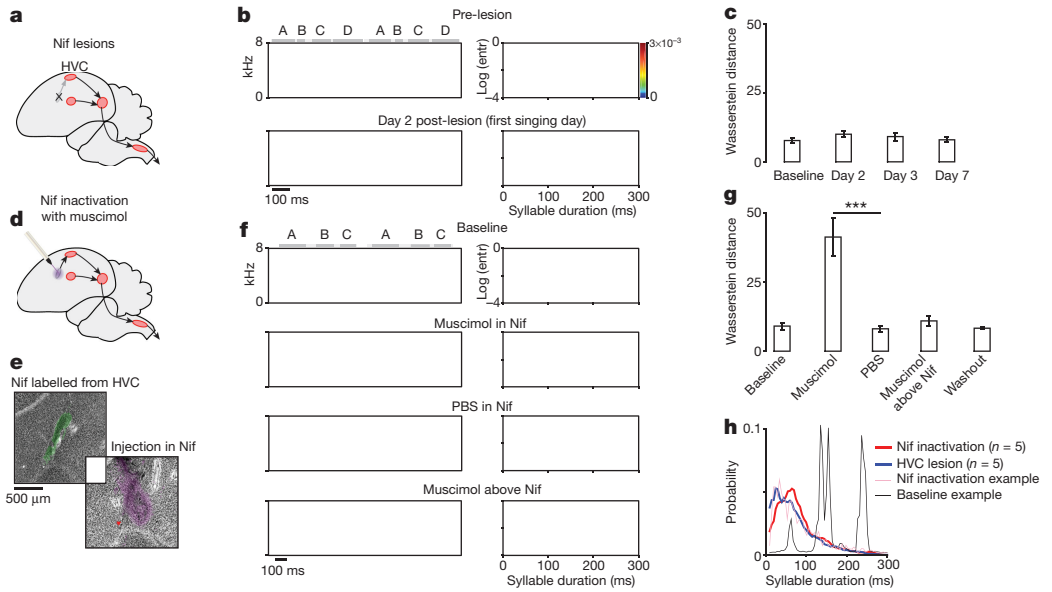

Figure 2 | Transient inactivations of Nif severely degrade adult zebra finch song, while permanent lesions have no noticeable effect when singing resumes two days later. a, Schematic of the song control circuit (red nuclei). Nif, a sensorimotor nucleus that inputs to HVC, was lesioned bilaterally ($n = 5$ birds). **b**, Left, spectrograms show two song motifs (syllables ABCD) from an example bird before (top), and after (bottom) bilateral Nif lesion. Right, joint entropy-duration distributions for song syllables uttered before and two days after the lesion. Letters denote syllables in the bird's song motif. **c**, Summary statistics showing the difference (Wasserstein distance) between the joint entropy-duration distributions before and on different days after Nif lesions. 'Baseline' compares the distributions from two consecutive days of pre-lesion singing. **d**, Schematic showing bilateral Nif inactivation. **e**, Histological sections of Nif. Top, injection of cholera toxin into HVC retrogradely labels Nif (green). Bottom, fluorescent dextran co-injected with muscimol (violet). Red arrows denote estimated boundaries of Nif. **f**, Spectrograms (left) and syllable entropy-duration distributions (right) as in **b** for an example bird subjected to various injection protocols. **g**, Same as **c**, but comparing pre-injection songs to songs after muscimol/PBS injections ($n = 5$ birds). **h**, Syllable-duration distributions in Nif-inactivated birds compared to HVC-lesioned birds. Data for HVC-lesioned birds from ref. 26. Shown for comparison are the distributions for baseline and Nif inactivation for the bird in **f**. Error bars represent s.e.m. $***P < 0.001$.

downstream effects of local circuit manipulations. On the basis of our results and known anatomy (Fig. 2), we hypothesized that Nif inactivations perturb vocal output by removing excitatory input from HVC, thus compromising the function of this song-specialized premotor area[28].

Most lesion protocols require surgery, which suppresses singing for a day or two, exactly the timeframe during which we hypothesize that recovery in HVC function occurs. To monitor neural dynamics in HVC in the immediate aftermath of Nif lesions and to compare it to pre-lesion dynamics, we lesioned Nif in freely behaving birds while recording multi-unit neural activity in HVC[29]. Stimulation electrodes targeted to Nif were implanted together with recording probes in ipsilateral HVC (Fig. 3a; Methods). Nif was lesioned unilaterally by injecting 50 µA of current for 30–40 s ($n = 11$ birds; Fig. 3b). Nif was successfully ablated (>80% lesioned; Methods) in 4 out of 11 birds, and subsequent analysis was done on this cohort unless otherwise noted.

Spontaneous (that is, non-vocal) HVC activity was dramatically reduced immediately following the lesions, consistent with a sudden loss of excitatory input from Nif[30], but recovered in the ensuing hours (Fig. 3c). Singing, which was invariably interrupted by the electrical stimulation, resumed after 1.3 ± 0.9 h (Fig. 3c–e). A fraction of the initial post-lesion vocalizations were severely degraded and did not resemble pre-lesion song[18] (Fig. 3d, e and Extended Data Fig. 5). The effects were less severe than during bilateral Nif inactivation (Fig. 2f, g), probably reflecting bilateral control of zebra finch song[31].

For vocalizations that resembled pre-lesion song, neural activity was aligned to a common song template (Methods). Although song-aligned activity patterns were similar across renditions in the hours following Nif lesions, they were strikingly different from pre-lesion dynamics (Fig. 3f–h).

Despite the initial degradation of song and associated HVC dynamics, both gradually recovered (Fig. 3e–h). By the second day, the song was reliably back to pre-lesion form (Fig. 3e). Remarkably, the average song-aligned activity patterns in HVC also recovered their pre-lesion structure (Fig. 3f–h). By the third day, the residual difference was consistent with normal drift in the recordings. Interestingly, the temporal structure of song-aligned HVC activity recovered predominantly during the night, while song-related HVC power recovered during the day (Fig. 3i; Methods).

To assess the extent to which acute post-lesion changes in HVC dynamics were caused by removal of Nif input versus non-specific effects of the current injections, we quantified changes in song-related HVC dynamics as a function of Nif lesion size. We found the extent of Nif damage to be strongly correlated with changes in song-related HVC activity following lesions (Fig. 3j), consistent with the acute degradation of song and associated HVC activity being due to removal of Nif input to HVC.

Activity homeostasis explains functional recovery

The spontaneous and gradual recovery of HVC activity after Nif lesions (Fig. 3c, h) was suggestive of homeostatic regulation of neural activity[7–9]. To probe whether this could explain the observed song recovery, we modelled HVC as a synaptically connected chain of neurons (a 'synfire chain') that receives time-varying excitatory input from Nif[32,33] (Fig. 4a; Methods). The network generated stable propagation of synchronous spiking activity, much like what is assumed for HVC during singing[34]. Acute removal of Nif input prevented many neurons in the chain from reaching spiking threshold, causing activity propagation to slow and often stop prematurely (Fig. 4c, d). Homeostatic regulation of neural activity in the HVC network was implemented by adaptively adjusting either spiking threshold[35] (Fig. 4b), input resistance[36] or strength of synaptic inputs[37] (Extended Data Fig. 6) of individual HVC neurons (Methods). These mechanisms all had similar effects: increasing the probability of HVC spiking while speeding up chain propagation and decreasing the likelihood of early 'song' terminations (Figs 4b–d and Extended Data Fig. 6).

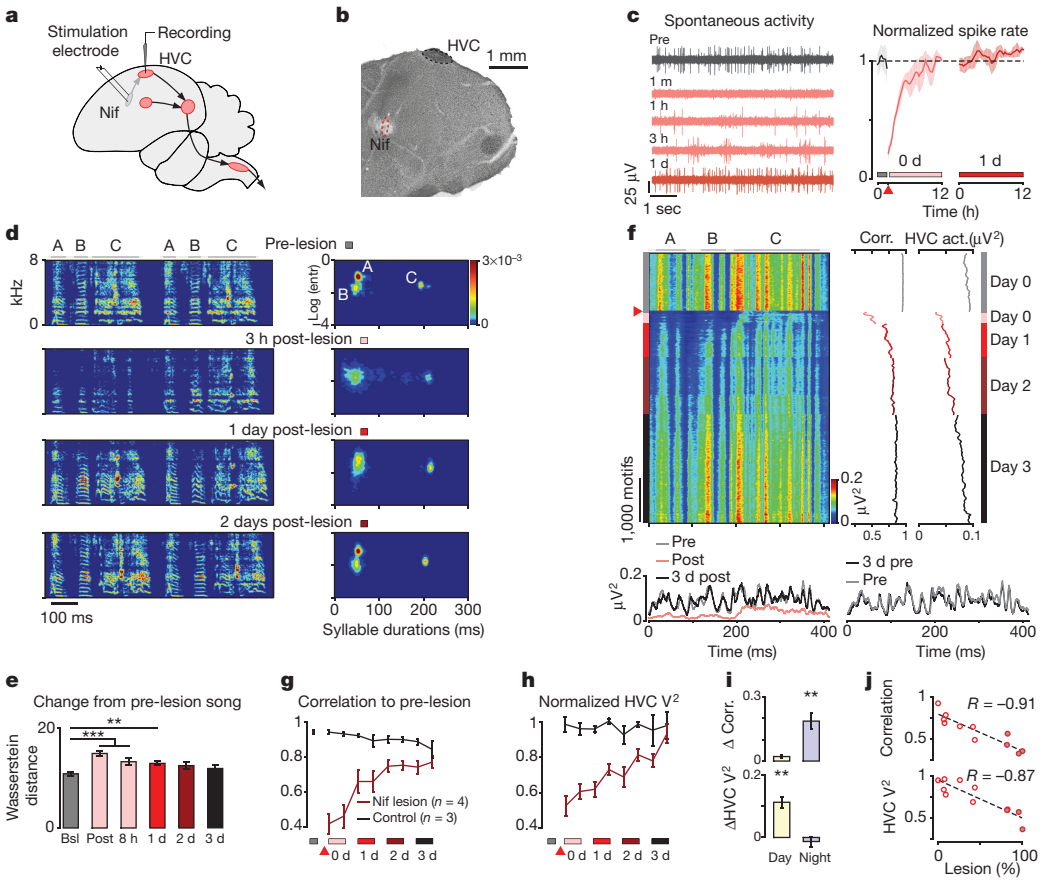

Figure 3 | Initial disruption and subsequent recovery in vocal performance and HVC dynamics following Nif lesions. a, Schematic of the experiment: lesioning Nif unilaterally while continuously recording neural activity from ipsilateral HVC. **b**, Histology of an electrolytic Nif lesion. **c**, Left, spontaneous activity in HVC before and at different time points after unilateral Nif lesion in an example bird. Right, recovery of spontaneous HVC activity normalized to pre-lesion rates averaged across Nif lesioned birds ($n = 4$) (lesion indicated by red arrow). Spontaneous activity recovered with a time constant of 3.4 ± 1.5 h. Shaded region denotes s.e.m. **d**, Representative spectrograms (left) and joint entropy-duration distributions (right) for songs of an example bird before and at different times after unilateral Nif lesion. **e**, Summary statistics showing the difference (Wasserstein distance) between the joint entropy-duration probability distributions before, and at different times after, unilateral Nif lesions. Baseline ('Bsl') compares the distributions from two consecutive days of pre-lesion singing. **f**, Recovery in song-related HVC dynamics following Nif lesion for the bird in **d**. Left, song-aligned neural power in HVC for song motifs uttered on the day of Nif lesion (red arrow) and until 3 days after. Middle, correlation between the song-aligned HVC activity pattern and the average pre-lesion activity pattern. Right, average neural power in HVC during singing. Bottom-left panel, average song-aligned neural activity right before and after the lesion, and 3 days later. Bottom-right panel, same as on the left, but showing normal drift in the neural recording over the 3 days preceding the lesion. **g**, Recovery in song-aligned HVC activity following unilateral Nif lesions measured as the Pearson's correlation to the average pre-lesion activity pattern and averaged across 4 birds (red trace, Methods). Data points correspond to the first and last batch of 25 song motifs on each day. The control trace (black) comes from recordings in 3 of the 4 lesioned birds, but before the Nif lesions, and represents the expected drift in HVC recordings. **h**, Similar to **g**, but showing recovery of the mean neural power in HVC during song, normalized to pre-lesion power. **i**, Recovery in HVC dynamics parsed by day (start to end of day-time singing) and night (end of singing on one day to start of singing the next), over the first 60 h post-lesion. Top, recovery in the correlation to pre-lesion HVC dynamics. Bottom, recovery of mean neural power. **j**, Correlation between song-aligned HVC activity before and immediately after Nif lesions (top), and the mean song-related neural power immediately after lesions normalized to pre-lesion values (bottom), as a function of the fraction of Nif lesioned. Grey-filled circles identify birds with >80% Nif lesions that were included in the summary analyses (**c**, **e**–**i**). Error bars represent s.e.m. $***P < 0.001$, $**P < 0.01$.

Given that HVC is known to control song timing[25], our simulations generated predictions for the temporal structure of song following Nif lesion (Fig. 4d). In agreement with these predictions, we found a transient increase in premature song terminations (Fig. 4e, f and Extended Data Fig. 5). Upon closer inspection, we also found that the song slowed down after lesion[18], only to recover in the ensuing days (Fig. 4f), again consistent with the qualitative predictions of our model. Though we cannot exclude other mechanisms, our network simulations are consistent with functional recovery after Nif lesions being due to homeostatic regulation of neural activity in HVC.

Discussion

Although efforts to understand the brain must necessarily rely on reductionist approaches, the simplifications and assumptions made in this pursuit must be scrutinized to prevent misleading conclusions. Given the increased reliance on transient circuit manipulations (for example, optogenetics, pharmacology, pharmacogenetics, cooling and transcranial magnetic stimulation) for localizing brain function, we tested whether behavioural effects induced by sudden activity perturbations reliably reflect the computations carried out in targeted areas. In two different systems, the deficits induced by transient manipulations seemingly overestimated the steady-state function of the examined circuits (Figs 1 and 2). This could be explained by the manipulations acutely affecting the independent functions of downstream circuits. We found that such off-target effects can resolve after the targeted area is permanently lesioned (Fig. 3). Importantly, the post-lesion recovery process did not require any renewed experience with the task, and was consistent with homeostatic regulation of neural activity (Fig. 4).

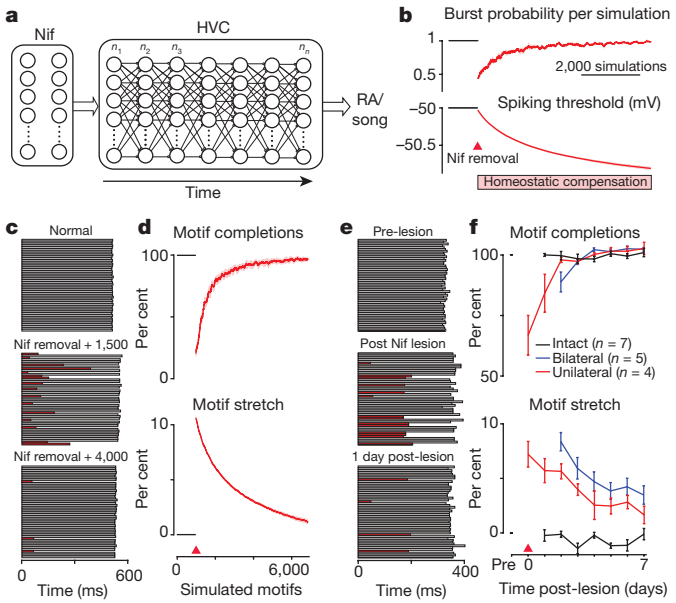

Figure 4 | Homeostatic regulation of spiking activity in HVC neurons can account for the functional recovery after Nif lesions. a, HVC is modelled as a chain of synchronously firing neurons, with each neuron receiving a different time-varying input from Nif (Methods). **b**, Top, Nif removal reduces the probability of spiking during simulated 'song' in a model neuron (from the 40th node). Bottom, homeostatic regulation of neural activity is implemented by adaptively adjusting the spiking threshold (Methods). **c**, **d**, Behaviour of the HVC model network after removal of Nif input and subsequent homeostatic regulation of single neuron firing rates. **c**, Fifty simulated 'songs' before and at two different times (1,500 and 4,000 simulations respectively) after Nif removal. Completed 'songs' in grey; truncated ones in red. **d**, Top, fraction of simulations for which activity in the model HVC network propagated to the end. Bottom, average duration of a full chain-propagation as a function of homeostatic recovery. **e**, **f**, Similar to **c** and **d**, respectively, but for birds with unilateral ($n = 4$) and bilateral ($n = 5$) Nif lesions. **f**, Motif completion rates (top) and tempo (bottom) relative to pre-lesion baseline. Data for intact birds come from a subset of the birds that were later lesioned. Error bars represent s.e.m.

Discrepancies between acute and chronic behavioural effects of targeted inactivations/lesions have been recognized in other contexts[10–12,14]. Acute effects are almost invariably more severe, a discrepancy typically explained by the brain adaptively compensating for lost function after lesions[15]. By not allowing time for experience-dependent compensation, transient circuit manipulations are seen as overcoming this 'caveat' of lesions. However, if the goal is to assign computations and memory functions to specific brain areas, our results suggest that transient circuit manipulations may have their own interpretive difficulties that stem from acute effects on the independent functions of non-targeted circuits.

That the function of a circuit can be sensitive to sudden perturbations in chronically non-essential inputs is not surprising. The brain—a finely tuned, complex, and heavily interconnected dynamical system—operates in a fairly limited dynamic regime[38], making it plausible that local circuit perturbations could interfere with the dynamics and independent functions of remote circuits[39]. For example, sudden removal of permissive inputs could tilt a network's excitatory-inhibitory balance[40], thus compromising its function[41]. This is seemingly what happens to HVC after Nif is silenced. Loss of excitatory input from Nif causes an acute decrease in the activity of HVC neurons[30], rendering the network incapable of producing its normal output (Figs 3f, g and 4).

The intricacies of dissecting interconnected biological networks and assigning functions to discrete nodes in those networks have been recognized in other contexts, including genetic and molecular networks[42]. In such studies, the distinction between permissive and instructive functions is routinely made[43,44]. Our results suggest that a similar distinction should be considered when interrogating the role of neural circuits in behaviour[45], with a circuit being classified as 'permissive' if its activity is acutely required for the expression of a behaviour without providing essential information for any of the underlying computations or memories. In contrast, a brain area should be considered 'instructive' if it contributes essential information or computation not otherwise available to the system implementing the behaviour.

Although the behavioural effects of sudden activity perturbations may not reliably reflect the steady-state function(s) of a circuit, lesions can, in certain cases at least, contribute additional insight. Permanent silencing of Nif and motor cortex suggested that the capacity of these brain areas to influence the respective skills we study—evident from transient manipulations—is not exercised under normal conditions, consistent with permissive roles. That Nif and motor cortex have access to the essential control circuits likely reflects instructive roles for these brain areas in behavioural processes that we did not test. Nif, for example, provides early auditory priming of HVC essential for imitative song learning[22], while motor cortical input to subcortical motor circuits is required for the initial acquisition of the skills we train[16] and for modulating other low-level motor behaviours[46].

Importantly, neural circuit function acutely compromised by sudden changes in permissive input can recover after those inputs are permanently silenced. Both skills we studied recovered after lesions without any task-specific practice, suggesting largely spontaneous recovery processes. Although the mechanisms that underlie such recovery will need to be further examined, our results are consistent with a role for homeostatic regulation of neural activity[7–9] (Fig. 4 and Extended Data Fig. 6). A similar recovery to the one we observed in HVC of songbirds (Fig. 3) has been described for the network underlying the pyloric rhythm in crustaceans[6], where homeostatic regulation of neuronal dynamics is thought to underlie the recovery of circuit function after removal of permissive or modulatory input[5].

Interestingly, we found that the structure of song-aligned HVC activity recovered predominantly overnight, while overall HVC power recovered during the day (Fig. 3i). This dissociation is consistent with the synaptic homeostasis hypothesis of sleep[47] that posits synaptic potentiation during wakefulness and synaptic rescaling and memory consolidation during sleep. Our results suggest that sleep not only consolidates activity patterns associated with recent experiences[48], but may help restore previously established circuit dynamics, and could hence promote functional recovery after brain lesions[49].

As in our experimental animals, patients with lesions to motor-related brain areas have motor deficits that resolve in the days and weeks following the injury[50]. Aspects of this recovery are thought to be independent of rehabilitation[13], suggesting spontaneous processes at work. Diaschisis is a broad clinical term referring to the temporary effects of focal brain lesions on remote brain areas[3], yet the underlying mechanisms remain poorly understood[41]. Our results suggest that focal brain lesions can affect neural dynamics and function in remote brain areas, and that homeostatic regulation of neuronal dynamics may help resolve such acute effects, thus contributing to functional recovery after brain injury.

Online Content Methods, along with any additional Extended Data display items and Source Data, are available in the online version of the paper; references unique to these sections appear only in the online paper.

Received 17 June; accepted 9 November 2015.
Published online 9 December 2015.

1. Lomber, S. G. The advantages and limitations of permanent or reversible deactivation techniques in the assessment of neural function. *J. Neurosci. Methods* **86,** 109–117 (1999).
2. Zhang, F., Aravanis, A. M., Adamantidis, A., de Lecea, L. & Deisseroth, K. Circuit-breakers: optical technologies for probing neural signals and systems. *Nature Rev. Neurosci.* **8,** 577–581 (2007).
3. Carrera, E. & Tononi, G. Diaschisis: past, present, future. *Brain* **137,** 2408–2422 (2014).

4. Honey, C. J. & Sporns, O. Dynamical consequences of lesions in cortical networks. *Hum. Brain Mapp.* **29,** 802–809 (2008).
5. Golowasch, J., Casey, M., Abbott, L. F. & Marder, E. Network stability from activity-dependent regulation of neuronal conductances. *Neural Comput.* **11,** 1079–1096 (1999).
6. Thoby-Brisson, M. & Simmers, J. Long-term neuromodulatory regulation of a motor pattern-generating network: maintenance of synaptic efficacy and oscillatory properties. *J. Neurophysiol.* **88,** 2942–2953 (2002).
7. Keck, T. *et al.* Synaptic scaling and homeostatic plasticity in the mouse visual cortex *in vivo*. *Neuron* **80,** 327–334 (2013).
8. Marder, E. & Goaillard, J.-M. Variability, compensation and homeostasis in neuron and network function. *Nature Rev. Neurosci.* **7,** 563–574 (2006).
9. Turrigiano, G. G. Homeostatic plasticity in neuronal networks: the more things change, the more they stay the same. *Trends Neurosci.* **22,** 221–227 (1999).
10. Bender, D. B. & Baizer, J. S. Saccadic eye movements following kainic acid lesions of the pulvinar in monkeys. *Exp. Brain Res.* **79,** 467–478 (1990).
11. Wilke, M., Turchi, J., Smith, K., Mishkin, M. & Leopold, D. A. Pulvinar inactivation disrupts selection of movement plans. *J. Neurosci.* **30,** 8650–8659 (2010).
12. Talwar, S. K., Musial, P. G. & Gerstein, G. L. Role of mammalian auditory cortex in the perception of elementary sound properties. *J. Neurophysiol.* **85,** 2350–2358 (2001).
13. Van Peppen, R. P. *et al.* The impact of physical therapy on functional outcomes after stroke: what's the evidence? *Clin. Rehabil.* **18,** 833–862 (2004).
14. Newsome, W. T. & Pare, E. B. A selective impairment of motion perception following lesions of the middle temporal visual area (MT). *J. Neurosci.* **8,** 2201–2211 (1988).
15. Maldonado, M. A., Allred, R. P., Felthauser, E. L. & Jones, T. A. Motor skill training, but not voluntary exercise, improves skilled reaching after unilateral ischemic lesions of the sensorimotor cortex in rats. *Neurorehabil. Neural Repair* **22,** 250–261 (2008).
16. Kawai, R. *et al.* Motor cortex is required for learning but not for executing a motor skill. *Neuron* **86,** 800–812 (2015).
17. Immelmann, K. in *Bird Vocalizations* (ed. Hinde, R.A.) 61–74 (Cambridge Univ. Press, 1969).
18. Cardin, J. A. Sensorimotor nucleus NIf is necessary for auditory processing but not vocal motor output in the avian song system. *J. Neurophysiol.* **93,** 2157–2166 (2005).
19. Huber, D. *et al.* Multiple dynamic representations in the motor cortex during sensorimotor learning. *Nature* **484,** 473–478 (2012).
20. Peters, A. J., Chen, S. X. & Komiyama, T. Emergence of reproducible spatiotemporal activity during motor learning. *Nature* **510,** 263–267 (2014).
21. Martin, J. H. Autoradiographic estimation of the extent of reversible inactivation produced by microinjection of lidocaine and muscimol in the rat. *Neurosci. Lett.* **127,** 160–164 (1991).
22. Roberts, T. F., Gobes, S. M. H., Murugan, M., Ölveczky, B. P. & Mooney, R. Motor circuits are required to encode a sensory model for imitative learning. *Nature Neurosci.* **15,** 1454–1459 (2012).
23. Zhang, F., Wang, L.-P., Boyden, E. S. & Deisseroth, K. Channelrhodopsin-2 and optical control of excitable cells. *Nature Methods* **3,** 785–792 (2006).
24. Klapoetke, N. C. *et al.* Independent optical excitation of distinct neural populations. *Nature Methods* **11,** 338–346 (2014).
25. Long, M. A. & Fee, M. S. Using temperature to analyse temporal dynamics in the songbird motor pathway. *Nature* **456,** 189–194 (2008).
26. Aronov, D., Andalman, A. S. & Fee, M. S. A specialized forebrain circuit for vocal babbling in the juvenile songbird. *Science* **320,** 630–634 (2008).
27. Fee, M. S. & Scharff, C. The songbird as a model for the generation and learning of complex sequential behaviors. *ILAR J.* **51,** 362–377 (2010).
28. Simpson, H. B. & Vicario, D. S. Brain pathways for learned and unlearned vocalizations differ in zebra finches. *J. Neurosci.* **10,** 1541–1556 (1990).
29. Ali, F. *et al.* The basal ganglia is necessary for learning spectral, but not temporal, features of birdsong. *Neuron* **80,** 494–506 (2013).
30. Hahnloser, R. H. R. & Fee, M. S. Sleep-related spike bursts in HVC are driven by the nucleus interface of the nidopallium. *J. Neurophysiol.* **97,** 423–435 (2007).
31. Schmidt, M. F., Ashmore, R. C. & Vu, E. T. Bilateral control and interhemispheric coordination in the avian song motor system. *Ann. NY Acad. Sci.* **1016,** 171–186 (2004).
32. Long, M. A., Jin, D. Z. & Fee, M. S. Support for a synaptic chain model of neuronal sequence generation. *Nature* **468,** 394–399 (2010).
33. McCasland, J. S. Neuronal control of bird song production. *J. Neurosci.* **7,** 23–39 (1987).
34. Hahnloser, R. H., Kozhevnikov, A. A. & Fee, M. S. An ultra-sparse code underlies the generation of neural sequences in a songbird. *Nature* **419,** 65–70 (2002).
35. Watt, A. J. & Desai, N. S. Homeostatic plasticity and STDP: keeping a neuron's cool in a fluctuating world. *Front. Synaptic Neurosci.* **2,** 5 (2010).
36. van Welie, I., van Hooft, J. A. & Wadman, W. J. Homeostatic scaling of neuronal excitability by synaptic modulation of somatic hyperpolarization-activated I_h channels. *Proc. Natl Acad. Sci. USA* **101,** 5123–5128 (2004).
37. Turrigiano, G. G., Leslie, K. R., Desai, N. S., Rutherford, L. C. & Nelson, S. B. Activity-dependent scaling of quantal amplitude in neocortical neurons. *Nature* **391,** 892–896 (1998).
38. van Vreeswijk, C. & Sompolinsky, H. Chaotic balanced state in a model of cortical circuits. *Neural Comput.* **10,** 1321–1371 (1998).
39. London, M., Roth, A., Beeren, L., Häusser, M. & Latham, P. E. Sensitivity to perturbations *in vivo* implies high noise and suggests rate coding in cortex. *Nature* **466,** 123–127 (2010).
40. Shu, Y., Hasenstaub, A. & McCormick, D. A. Turning on and off recurrent balanced cortical activity. *Nature* **423,** 288–293 (2003).
41. Feeney, D. M. & Baron, J. C. Diaschisis. *Stroke* **17,** 817–830 (1986).
42. Phillips, P. C. Epistasis—the essential role of gene interactions in the structure and evolution of genetic systems. *Nature Rev. Genet.* **9,** 855–867 (2008).
43. Miyashita, T., Kubik, S., Lewandowski, G. & Guzowski, J. F. Networks of neurons, networks of genes: an integrated view of memory consolidation. *Neurobiol. Learn. Mem.* **89,** 269–284 (2008).
44. Shobe, J. The role of PKA, CaMKII, and PKC in avoidance conditioning: permissive or instructive? *Neurobiol. Learn. Mem.* **77,** 291–312 (2002).
45. Taha, S. A. & Fields, H. L. Inhibitions of nucleus accumbens neurons encode a gating signal for reward-directed behavior. *J. Neurosci.* **26,** 217–222 (2006).
46. Stoltz, S., Humm, J. L. & Schallert, T. Cortical injury impairs contralateral forelimb immobility during swimming: a simple test for loss of inhibitory motor control. *Behav. Brain Res.* **106,** 127–132 (1999).
47. Tononi, G. & Cirelli, C. Sleep function and synaptic homeostasis. *Sleep Med. Rev.* **10,** 49–62 (2006).
48. Walker, M. P. & Stickgold, R. Sleep-dependent learning and memory consolidation. *Neuron* **44,** 121–133 (2004).
49. Siccoli, M. M., Rölli-Baumeler, N., Achermann, P. & Bassetti, C. L. Correlation between sleep and cognitive functions after hemispheric ischaemic stroke. *Eur. J. Neurol.* **15,** 565–572 (2008).
50. Levin, H. S. & Grafman, J. *Cerebral Reorganization of Function after Brain Damage* (Oxford Univ. Press, 2000).

Supplementary Information is available in the online version of the paper.

Acknowledgements We thank E. Soucy and J. Greenwood for technical assistance. We are grateful to M. Meister, J. Sanes, N. Uchida, K. Blum, A. Dhawale, M. Josch, A. Kampff, and E. Feinberg for their feedback on our manuscript. This work was supported by a McKnight Scholars Award to B.P.Ö., HSFP and EMBO fellowships to S.B.E.W., an NRSA fellowship to R.K., and a Rubicon fellowship from the Netherlands Organization for Scientific Research to S.M.H.G.

Author Contributions B.P.Ö. and T.M.O. designed the study with input from all authors. T.M.O. collected and analysed the data from songbirds with help from A.K. S.M.H.G. did initial pilot experiments in songbirds that inspired the study. C.P. implemented the HVC network model. S.B.E.W. performed the optogenetics experiments in rats and analysed the data. J.Y.R. and R.K. performed the pharmacological inactivation experiments in rats and analysed the data. B.P.Ö. supervised and coordinated the project. B.P.Ö., T.M.O., and S.B.E.W. wrote the paper with input from the other authors.

Author Information Reprints and permissions information is available at www.nature.com/reprints. The authors declare no competing financial interests. Readers are welcome to comment on the online version of the paper. Correspondence and requests for materials should be addressed to B.P.Ö. (olveczky@fas.harvard.edu).

METHODS

Animals. The care and experimental manipulation of all animals were reviewed and approved by the Harvard Institutional Animal Care and Use Committee. Experimental subjects were female Long Evans rats 3–8 months old at start of training ($n = 10$, Charles River) and adult male zebra finches between 92–205 days post-hatch ($n = 27$). Because the behavioural effects of our circuit manipulations could not be pre-specified before the experiments, we chose sample sizes that would allow for identification of outliers and for validation of experimental reproducibility. No animals were excluded from experiments post-hoc. The investigators were not blinded to allocation during experiments and outcome assessment, unless otherwise stated.

Behavioural training in rats. Ten rats were trained in the lever-pressing task as previously described[16]. Water-restricted animals were rewarded with water for pressing a lever twice with a prescribed interval between the presses (700 ms for 9 of the rats, 600 ms for one). All animals were trained using our fully automated home-cage training system[51]. Kinematic tracking of forepaw movements (Fig. 1d, g) was done as in ref. 16.

Motor cortex inactivations in rats. In rats ($n = 5$) that had reached asymptotic performance in our task[16], a craniotomy was made to access the caudal forelimb area of primary motor cortex (CFA) in the hemisphere contralateral to the paw most involved in the lever-press sequence. The centre of the CFA was estimated from stereotactic coordinates (+1.0 mm anterior, +3.00 mm lateral, with respect to bregma[52]). Kwik-Kast sealant (WPI) was applied to cover the exposed dura. In addition, a protective acrylic cap covering the craniotomy was attached with screws to three nuts secured to the skull with Metabond (Parkell). After recovering from surgery (10 days), animals were trained for at least one additional week to ensure that they were at their asymptotic performance levels.

On injection days, rats were lightly anaesthetized with 0.5–1.5% isoflurane and placed in a stereotax. Motor cortex was accessed by removing the custom-made protective cap and the Kwik-Kast plug covering the craniotomy. Muscimol (or PBS for control) was injected at the estimated centre of the CFA[52], 1.5 mm deep, in 9.2 nl increments every 10 s using a Nanoject (WPI). The craniotomy was resealed with Kwik-Cast and the protective cap reattached. The whole procedure took 15–30 min, and rats resumed normal behaviour a few minutes later. Training sessions started 1.5 h after the injections. 'Baseline' performance included sessions after the craniotomies but before injection. Experimental days alternated between saline and muscimol injections. To prevent any behavioural compensation in response to muscimol-induced performance deficits, injected animals were tested for only 10 min.

The dosing of muscimol was based on two criteria. (1) To allow comparisons with our lesion study[16], the direct effect of muscimol injections should be restricted to a volume of motor cortex equal to or smaller than what we lesioned in ref. 16 (Fig. 1c). (2) To quantify effects on kinematics and performance, drug dosing should not abolish task engagement. We injected increasing concentrations and volumes of muscimol in two rats, and found that relatively larger doses (200–400 nl of 25 mM muscimol) degraded performance to the point where animals quit the task (Supplementary Video 1).

We converged on a dose of 100 nl of 25 mM muscimol because it generally did not prevent engagement with the task and because we estimated that it affects a volume significantly smaller than what we lesioned in ref. 16. Our estimate of muscimol spread is bounded by previous studies that injected larger doses of muscimol[21,53] (1 μl of 2 and 9 mM, respectively) and showed affected volumes of ~4–14 mm^3. In comparison, our motor cortex lesions were larger than 23 mm^3 (ref. 16). We also injected 100 nl of 25 mM fluorescein in one animal using the same protocol as for the experimental animals, euthanizing it 1.5 h after the injection. Its brain was later sectioned, and the approximate spread of the dye visualized using fluorescence microscopy (Fig. 1c). One of the experimental animals had very severe performance deficits at our chosen dosing, preventing us from characterizing the behavioural effect (that is, very few successful trials). In this animal we reduced the concentration to 1 mM, at which the task engagement was robust but the performance still affected (Fig. 1d).

Optogenetic stimulation. *Viral injections.* Adeno-associated virus (AAV2/8-hSyn-FLEX-ChrimsonR-tdTomato, UNC vector core[24]; titre: 5×10^{12} vector genomes (vg) per ml) was injected into the forelimb motor cortex of isoflurane anaesthetized rats ($n = 5$) through multiple small craniotomies (A/P, M/L: +1, ±2; +1, ±4; +1.5, ±2.75; +2.25, ±2.5; +3, ±2, coordinates relative to bregma). Injections were done in 9.2 nl increments while slowly moving the injection-pipette (Nanoject) from a depth of 1.5 mm to 0.7 mm for a total volume of 0.4 μl per site and 2 μl per hemisphere (Extended Data Fig. 1a). Animals were allowed to recover for 5 days before starting behavioural training.

LED implant and stimulation. Once animals reached asymptotic performance on our task[16], they underwent a second surgery to implant a custom-built device for optogenetic stimulation (Extended Data Fig. 1c). The device consisted of a red light-emitting diode (LED) ($\lambda = 615$ nm, 110 mW output power, XLAMP XPC LED RD-ORANGE, Cree) on a printed circuit board, powered by two coin-cell batteries (CR2032). An infrared (IR)-sensitive photodiode was used to wirelessly control the LED. After device implantation and recovery, animals resumed behavioural training. An IR light-source placed on top of the training cage was activated to trigger the LED for the duration of the optogenetic stimulation (1 s or 50 ms, continuous light). Stimulation trials were at least 10 s apart to allow the batteries of the LED to recover. Between stimulation trials, rats performed a varying number of non-stimulated trials (range: 0–5), resulting in ~30% of the trials being 'stimulated'. Optogenetic stimulation was repeated for several sessions (5–12). Batteries were changed daily.

Functional verification. To characterize the effects of optogenetic stimulation on motor cortex activity, acute electrophysiological recordings were done after termination of the behavioural experiments in two of the rats. The animals were anaesthetized and placed in a stereotactic frame. The implanted LED device was carefully removed to expose the previous craniotomy. Using a custom-built recording setup and silicon probes (Buzsaki-64, Neuronexus), we recorded single-unit activity in motor cortex below the craniotomy. The removed LED device was placed next to the silicon probe above the craniotomy. Once stable units were detected, we triggered the LED and illuminated motor cortex for 1 s (30 trials). Recordings were performed at multiple depths (0.1 mm to 2.5 mm). Units were classified as light responsive if at least two consecutive bins of 5 ms during the first 200 ms of illumination had a significant z-score (compared to 1 s of baseline before light onset). These included units with long onset latencies (>10 ms), consistent with indirect activation (Extended Data Fig. 1b). The relatively high number of light responsive units (69 ± 3%), compared to the number of cells counted as infected by immunohistochemistry 31 ± 2%; see below), is likely due to such indirect effects. Moreover, many of the recorded light-responsive cells were only identified during stimulation, further biasing our results to responsive cells.

Histological verification. At the end of the experiments, animals were transcardially perfused with PBS and subsequently fixed with 4% paraformaldehyde (PFA) in PBS. Brains were removed and post-fixed for at least 24 h. Brains were sliced coronally (thickness: 80 μm) and immunohistochemistry performed to determine the AAV injection site and extent of the transfection (Extended Data Fig. 1a). Slices were blocked (1% BSA, 0.3% Triton in PBS) at room temperature and incubated with anti-RFP (chicken, 1:1,000, Millipore, AB3528) and anti-NeuN (mouse, Millipore, MAB377) primary antibodies in blocking buffer for 48 h at 4 °C. After washing, slices were incubated with anti-chicken-Alexa 568 (goat, 1:1,000, Life Technologies, A-11041) and anti-mouse-Alexa 647 (goat, 1:1000, Life Technologies, A-31625) over night at 4 °C. Slices were mounted and imaged using a Zeiss Axio Scan Z1 Slide Scanner for overview images and an Olympus FluoView FV1000 confocal microscope for high-resolution images. We verified the targeting and spread of all injections based on the fluorescent signal and determined the extent of the AAV injections in a subset of animals (8.2 mm^3 ± 1.3 mm^3; $n = 2$ rats). In addition we chose 4 regions of interest (size 635 × 635 μm) and counted the number of infected cells relative to the number of neurons ($NeuN^+$ cell) to determine the fraction of infected cells (31 ± 2%; $n = 2$ rats). Histology was done blind to the outcome of the experiment.

Data analysis for rat experiments. To assess the behavioural effects of the different injections in the acute inactivation experiments, we measured performance relative to 'baseline' training sessions after the craniotomies but before any injections. To standardize analysis across experimental conditions (muscimol, PBS, or baseline), we only included data from the first 10 min of each session, matching the duration of the muscimol sessions. For the optogenetic stimulation experiments, 'baseline' was defined as the non-stimulated trials in the same sessions. The number of sessions for each condition ranged from 1–3 (injections) and 5–12 (optogenetic stimulations). Data from training sessions of a given condition were pooled for each animal. To quantify behavioural performance, the fraction of trials with an inter-press interval (IPI) within 20% of the target IPI was calculated. Data on motor cortex lesioned animals presented for comparisons in Fig. 1e comes from previously published experiments[16], and includes sessions from the second week of post-lesion training.

Zebra finch experiments. All birds were obtained from the Harvard University zebra finch breeding facility and housed on a 13:11 h light/dark cycle in acoustic isolation with food and water provided ad libitum.

Pharmacological lesions. Birds ($n = 5$) were anaesthetized with isoflurane. Nif was localized antidromically by electrical stimulation in HVC[29]. Bilateral Nif lesions were made by injecting the excitotoxin *N*-methyl-DL-aspartic acid (NMA, 4%) into each hemisphere using a Nanoject (WPI). In initial experiments, a single 27 nl bolus of NMA was injected into the centre of Nif. Though this volume produced complete bilateral Nif lesions in one animal, we found that complete lesions were more reliably produced by injecting two boluses of 18 nl (for a total of 36 nl) 200 μm apart along the anterior-posterior axis. We report on the five animals that had 100%

bilateral Nif lesions, determined by post-hoc histological inspection (see below, Extended Data Fig. 3b). One of these received 27 nl and 4 received 36 nl injections.
Reversible inactivations. Birds ($n = 5$) were anaesthetized and Nif identified as described above. Craniotomies over Nif were covered with artificial dura (Body Double Fast; Smooth-On, Inc.) and head screws were attached to the skull with dental cement as previously described[54]. Following post-surgical recovery, awake birds were placed in a foam restraint and head-fixed to a stereotax for ~10 min each morning for 10–14 days to desensitize them to handling and restraint. Following the desensitization training, all birds reliably sang within 30 min of the restraint. In the morning of experimental days, muscimol (27 nl, 50 mM) or PBS (27 nl) was injected bilaterally as described in the text. In two birds that routinely sang within 10 min of drug administration, we also injected a smaller dose (9 nl) of muscimol into Nif to additionally verify that song degradation was due to direct inactivation of Nif (Extended Data Fig. 4b).

We note that a previous study aimed at reversibly inactivating Nif in adult songbirds failed to show any obvious effect on song structure[55], but conflicting results from experiments in juvenile birds and methodological uncertainties regarding drug injection volumes in adult birds make its conclusions tentative. This previous report notwithstanding, all our muscimol injections into Nif produced similarly severe song degradation (Fig. 2f and Extended Data Fig. 4b).
Implantation of recording and stimulation device. Zebra finches ($n = 11$) were anaesthetized with isoflurane and placed in a stereotax. HVC was identified by antidromic stimulation from Area X as previously described[29]. Nif was similarly identified by stimulating in HVC. For birds targeted for electrolytic Nif lesions, we placed either a monopolar stimulating electrode at the dorsal-posterior edge of Nif ($n = 8$ birds) or a bipolar stimulating electrode straddling Nif in the medial-lateral plane ($n = 3$ birds). A custom recording array (3 channels; 100 kΩ) was implanted in the hemisphere ipsilateral to the Nif-stimulating electrode and within the identified boundaries of HVC as previously described[29]. All birds exhibited normal song output within 7 days of surgery. Following completion of the experiment, animals were euthanized, their brains collected, and the placement of recording electrodes and extent of lesions confirmed histologically.
Neural and behavioural recordings. Sound and neural activity were recorded using a custom LabVIEW application (National Instruments) as previously described[29]. Multi-unit neural activity was recorded from up to three sites in HVC (~250 μm spacing) for three to four weeks per bird. Because stability of the neural recordings is crucial for estimating recovery in HVC dynamics, analysis was done on data collected at the most stable recording site in each bird (determined pre-lesion), though we note that the trends were similar across all channels.
Electrolytic lesions. Electrolytic lesions of Nif were made in the right hemisphere by passing 50 μA of monophasic current through the stimulating electrode for 30–40 s. Current injections started while birds were singing, and in all cases immediately terminated song output. Lesion extent was estimated post-hoc as described below.
Histological verification of lesions and inactivations. At the end of the experiments, birds were anaesthetized with natriumpentobarbital (Nembutal, IM) and transcardially perfused with PBS, followed by fixation with 4% PFA in PBS. Brains were removed and post-fixed in 4% PFA overnight. Parasagittal sections (75 μm) were cut on a Vibratome (Leica), mounted, and stained with cresyl violet to reconstruct the location of implanted electrodes and lesions (ImageJ). Identification of the injection sites for the muscimol inactivations and circuit tracings were done in alternate brain slices by fluorescence microscopy (Fig. 2e and Extended Data Fig. 4a). Histology was done blind to the identity of the animals.

Nif was identified based on regions of stronger staining and higher cell density than surrounding areas and were additionally guided by proximate anatomical landmarks (for example, HVC, the lamina mesopallialis and the lamina pallio-subpallialis).
Lesions. Location and size of the lesions were determined by estimating the extent of necrotic tissue (that is, loss of neurons and gliosis) in photomicrographs of cresyl violet stained sections as previously described[22]. Lesion size was expressed as a percentage of estimated Nif size, measured in intact controls ($0.035 \pm 0.001\ mm^3$, $n = 4$ birds). In pharmacologically lesioned birds, 100% of Nif was lesioned (Extended Data Fig. 3b). In electrolytically lesioned birds, 0–100% of Nif was lesioned (Fig. 3j).
Inactivations. Fluorescent dye-conjugated dextrans ($0.5\ mg\ ml^{-1}$ Alexa 594; Invitrogen) were co-injected with the final injection of muscimol for post-hoc verification of the injection site (Fig. 2e and Extended Data Fig. 4a). Fluorescence images of the sections were superimposed on those of their adjacent cresyl violet sections (Adobe Photoshop) to determine locations of fluorescence in relation to Nif. All injection sites were found to be within the target nucleus (Extended Data Fig. 4a).
Neural circuit tracing. To visualize Nif (Fig. 2e and Extended Data Fig. 3a), fluorescent dye-conjugated cholera toxin subunit B ($1\ mg\ ml^{-1}$, Alexa 488; Invitrogen) was injected into HVC in 2 birds (83 nl per hemisphere). Twenty-one days after surgery, the animals were euthanized, perfused, and their brains fixed, sectioned, and mounted. Photomicrographs of fluorescent sections were overlaid on those of adjacent cresyl violet sections (Adobe Photoshop) to determine the location of fluorescence in relation to anatomical landmarks and density of cell bodies.
Data analysis of song. *Syllable segmentation and annotation.* Raw audio recordings were segmented into syllables as previously described[29]. Spectrograms were calculated for all prospective syllables, and a neural network (5,000 input layer, 100 hidden layer, 3–10 output layer neurons) was trained to identify syllable types using a test data set created manually by visual inspection of song spectrograms. Accuracy of the automated annotation was verified by visual inspection of a subset of syllable spectrograms.
Syllable feature quantification. All non-call vocalizations were characterized by their duration and mean Wiener entropy—both robust acoustic features that are tightly controlled in adult zebra finch song[56]. Syllable durations were estimated from threshold crossings of the acoustic power as previously described[29]. Wiener entropy, a measure of acoustic randomness, was calculated using Sound Analysis for MATLAB[57] for 10 ms time windows, advancing in steps of 1 ms, such that entropy was computed for every millisecond. The entropy measurements were averaged across the syllable and log-transformed. On this scale, the Wiener entropies of white noise and of a pure tone are zero and minus infinity, respectively.
Duration probability distributions. Histograms (1.25 ms bins) of syllable durations produced within 1 h of muscimol/PBS injections were generated for each experiment, normalized by total sample counts, averaged across 2–4 experiments within a bird, and then averaged across birds. Data from HVC-lesioned birds, provided by the authors of ref. 26, was recorded on the first day of singing after lesion (2–7 days after surgery) and analysed similarly. Mean duration distributions for all conditions were smoothed with a sliding boxcar window (7-bin width, 1-bin advance).
Entropy-duration joint probability distributions. Two-dimensional histograms, showing the joint distributions of syllable duration and Wiener entropy, were created with bins of width 1.25 ms (duration axis; range: 0–300 ms) and 0.025 (log Wiener entropy axis; range: −4–0). The histogram was normalized by total sample counts to construct an empirical probability distribution. Because these empirical distributions were sparsely sampled, we estimated the true probability distribution by smoothing the empirical distribution with a point-spread function (2D Gaussian; width: 7 bins; sigma: 3 bins). Distributions were calculated for vocalizations produced during the following time windows. Bilateral lesion experiments: the first 2 h of singing each day; inactivation experiments: 2 h before (pre), 1 h after (post), and 6–8 h after (washout) injection; unilateral lesion: the first 2 h of singing each day, the first hour of post-lesion singing, and the last 4 h of singing on the day of lesion.
Distribution similarity measurement. To quantify changes in song elements, we calculated the first Wasserstein distance, a common metric of the difference in probability distributions, between syllable entropy-duration distributions for songs produced at different time points or under various experimental conditions (see text). We used an implementation in MATLAB and C available at (http://www.ariel.ac.il/sites/ofirpele/FastEMD/). Distances between bins were Euclidean. Calculations were based on 50,000 samples drawn from the entropy-duration probability distributions and reported in figures as the mean distance per sample.
Motif completion rate. For each bird, a 3–5 syllable dominant song motif was identified by visual inspection of spectrograms. Motif completion rates (MCR) were calculated as:

$$\mathrm{MCR} = \frac{\text{Number of utterances of complete motifs}}{\text{Number of utterances of the first syllable in the motif}}$$

For all birds, motif completion rates were calculated for the first two hours of singing per day; for unilaterally lesioned birds, rates were also calculated for the first hour of singing following lesion. 'Intact' motif completion rates (Fig. 4f) were based on a subset of the lesioned birds (four from the 'bilateral'; three from 'unilateral' group) but collected 1–2 weeks before the Nif lesions. Data from each bird was normalized to pre-lesion motif completion rates for comparison across animals. See Extended Data Fig. 5 for examples of truncated motifs.
Motif duration stretch. The durations of the dominant song motifs were calculated as previously described[29] for interval durations. For all birds, the mean motif duration was calculated for 100 consecutive renditions, taken at the same time each day (~1 h after lights on in the morning). For unilaterally lesioned birds, the mean duration was also calculated for the first 100 identifiable motifs produced immediately after lesion. As noted above, 'intact' data were collected from birds that were later lesioned. Motif durations were normalized to pre-lesion values for comparison across animals. See Extended Data Fig. 5 for examples of aligned and excluded vocalizations.
Data analysis of neural recordings. *Spontaneous activity.* To record spontaneous HVC activity, minute long recordings were made every 15 min. These recordings

were bandpass filtered (1–5 kHz; 2-pole Butterworth; zero-phase) and segments within 500 ms of vocalization-related activity were marked for exclusion from subsequent analysis. Individual spikes were detected by an amplitude threshold set to 3–8 standard deviations of the estimated noise in the recordings. For each bird, the spontaneous firing rates were normalized to the mean firing rate in the two hours before lesion. Shown in Fig. 3c is the across-bird mean and standard error, smoothed with a sliding boxcar window (5 bin width, 1 bin advance).

Alignment of the neural recordings to song. A dynamic time warping (DTW) algorithm was used to align individual song motifs to a common template as previously described[29]. The warping path derived from this alignment was then applied to the corresponding HVC recordings with a premotor lead of 35 ms[29]. The aligned neural traces were squared (to calculate signal power) and smoothed (5 ms boxcar window, 1 ms advance).

HVC activity correlation. The recovery of temporal dynamics in HVC was calculated as the Pearson's correlation between the song-aligned neural power immediately before lesion and the same at different times after lesion. The running correlation in Fig. 3f shows Pearson's correlation between the mean song-aligned activity pattern of pre-lesion songs on the day of lesion and the mean activity patterns in a sliding window of 25 song motifs. The pre-lesion data point in Fig. 3g represents the correlation between the mean power envelopes for two consecutive blocks of 25 motifs recorded immediately before lesion. Normal drift in the song-related HVC signal ('control') was calculated similarly.

HVC mean power. The mean HVC power was calculated per motif and averaged over the 25-motif windows as described above for the correlation. For analyses pooled across birds, mean HVC power was normalized to the pre-lesion value.

Day versus night recovery. Recovery of HVC activity in the first 60 h following lesion, during which most of the post-lesion recovery occurred, was parsed into 3 day-time and 2 night-time intervals. Daytime recovery was calculated as the change in correlation to pre-lesion activity (or normalized mean power) between the first 25 motifs in the morning (or immediately following lesion) and the last 25 motifs that evening; night-time recovery is the change between the last 25 motifs of the day and the first 25 of the subsequent morning.

Modelling. *Network architecture.* On the basis of previous experimental findings[32,34], we modelled the HVC network as a synfire-chain of bursting neurons. The model consisted of 1,200 integrate-and-burst neurons organized into 80 nodes. Each of the 15 neurons in a node projected to all neurons in the next node, forming a chain topology.

The subthreshold membrane potential of the i^{th} neuron, V_i, obeys:

$$C\frac{dV_i}{dt} = -g_L(V_i - V_L) + I_{syn,i} + I_{Nif,i} + \sqrt{\tau_\eta}\sigma\eta_i(t)$$

where $C = 1\,\mu\text{F/cm}^2$ is the membrane capacitance, $g_L = 0.1\,\text{mS/cm}^2$ is the leak conductance, $V_L = -60\,\text{mV}$ is the leak potential, $I_{syn,i}$ is the synaptic input, $I_{Nif,i}$ represents external input to the HVC neurons from Nif, $\eta_i(t)$ is a zero-mean Gaussian white noise with covariance $\langle\eta_i(t)\eta_i(t')\rangle = \delta(t-t')$, $\tau_\eta = 10\,\text{ms}$ and $\sigma = 200\,\text{nA/cm}^2$. The synaptic input is given by $I_{syn,i}(t) = W\sum_j M_{ij}\sum_{k,\, t_j^k<t}\varepsilon(t-t_j^k)$, where t_j^k denotes the k^{th} spike of j^{th} neuron, $\varepsilon(t) = \Theta(t)e^{-t/\tau_s}$ with $\Theta(t)$ being the step function and $\tau_s = 5\,\text{ms}$, $W = 87\,\text{nA/cm}^2$ and M_{ij} is 1 for synapses from a neuron j to the neurons i in the next node and 0 otherwise. The Nif input is a different waveform for each HVC neuron and does not change across simulations. The waveforms were randomly generated by simulating an Ornstein-Uhlenbeck process with an autocorrelation time scale of 50 ms, starting from a random initial point. Noise and drift were chosen such that the resulting waveforms had a mean of $97\,\text{nA/cm}^2$ and standard deviation of $53\,\text{nA/cm}^2$. When the membrane potential of the integrate-and-burst neuron reaches threshold, $V_{th} = -50\,\text{mV}$, the neuron emits 4 spikes with 2 ms intervals, modelling the bursts generated by calcium spikes in RA-projecting HVC neurons[32,58], and the membrane potential is reset to $V_R = -55\,\text{mV}$ after a refractory period of 4 ms. Chain propagation was started by a 5 ms pulse input with magnitude $6.7\,\mu\text{A/cm}^2$ to the neurons in the first node. The parameters of the model were chosen to approximate the results of our experiments. Some of these parameters were subject to change as explained below.

Homeostatic regulation of neural activity. We implemented three different homeostatic plasticity rules, each of which can adaptively modify the excitability of HVC neurons.

Rule 1: if during a simulated chain propagation a neuron did not spike, its spiking threshold decreased by 1 μV. If the neuron produced more than 8 spikes or 2 bursts, the threshold increased by 1 μV. This rule is used in Fig. 4 and Extended Data Fig. 6a. Such homeostatic changes in spiking thresholds have been observed in experiments[35].

Rule 2: if during a simulated chain propagation a neuron did not spike, the leak conductance of the neuron decreased by $0.1\,\mu\text{S/cm}^2$. If the neuron produced more than 8 spikes or 2 bursts, the leak conductance increased by $0.1\,\mu\text{S/cm}^2$. This rule amounts to changing the neuron's input resistance, defined as the change in membrane potential in response to injected current, divided by the current. This rule is used in Extended Data Fig. 6b. Homeostatic changes to input resistance have also been observed in experiments[36].

Rule 3: if during a simulated chain propagation a neuron did not spike, all synaptic weights to that neuron increased by $6.7\,\text{pA/cm}^2$. If the neuron produced more than 8 spikes or 2 bursts, the synaptic weights decreased by $6.7\,\text{pA/cm}^2$. This rule is used in Extended Data Fig. 6c. Activity-dependent homeostatic changes to a neuron's synaptic inputs have been observed in experiments, for example, in cortical neurons[37].

In Fig. 4 and Extended Data Fig. 6, a 'motif' was considered complete if at least one neuron in each of the 80 nodes produced a spike. Motif duration was calculated as the time from the propagation initiation until the average spike time of the neurons in the last node. We ran simulations with modified parameters to verify that our results presented in Fig. 4 were qualitatively robust.

Statistical analysis. All statistics on data pooled across animals is reported in the main text as mean ± s.d. and depicted in figure error bars as mean ± s.e.m. Where appropriate, distributions passed tests for normality (Kolmogorov–Smirnov), equal variance (Levene), and/or sphericity (Mauchly), unless otherwise noted. Multiple comparison corrected tests were used where justified. Statistical tests for specific experiments were performed as described below.

Fig. 1e. Comparison of fraction of trials with IPIs within 20% of the target for different experimental treatments ($n = 5$ rats). Mauchly's test indicated a violation of sphericity ($W = 0.134$, $P = 0.049$), and a Huynh-Feldt degrees of freedom correction was applied. Subsequent repeated-measures ANOVA revealed significant differences between the treatments ($F_{(1.17,4.59)} = 35.7$, $P = 0.002$). Post-hoc comparisons using Dunnett's test showed significant differences between PBS (control) and muscimol injections ($P = 0.0002$), but not between PBS and baseline ($P = 0.99$).

Fig. 1h. Effect of optogenetic stimulation of motor cortex on task performance. A two-tailed, paired t-test revealed significant differences in performance in the light off and light on conditions ($n = 5$ rats; $P = 3 \times 10^{-5}$).

Fig. 2c. Comparison of Wasserstein distances between joint entropy-duration distributions before and after bilateral Nif lesions ($n = 5$ birds). Repeated-measures ANOVA showed no significant difference on any day ($F_{(3,12)} = 2.21$, $P = 0.14$).

Fig. 2g. Same as Fig. 2c, but comparing pre-injection songs to songs after muscimol/PBS injections ($n = 5$ birds). Mauchly's test indicated a violation of sphericity ($W = 1.9 \times 10^{-4}$, $P = 0.014$), and a Huynh–Feldt degree of freedom correction was applied. Subsequent repeated-measures ANOVA revealed significant differences between the treatments ($F_{(1.36,5.43)} = 19.7$, $P = 0.004$). Post-hoc comparisons using Dunnett's test showed significant differences between PBS (control) and muscimol injections ($P = 1 \times 10^{-5}$); no other condition significantly differed from PBS ($P > 0.92$).

Fig. 2h. Comparison of the syllable duration distributions following HVC lesions ($n = 5$ birds) and Nif inactivations ($n = 5$ birds). A Kolmogorov–Smirnov test on the mean distribution across animals showed no significant differences ($P = 0.24$).

Fig. 3e. Comparison of Wasserstein distances between joint entropy-duration distributions before and after unilateral lesions to Nif ($n = 4$ birds). Repeated-measures ANOVA revealed that lesions produced significant differences in song structure ($F_{(5,15)} = 17.7$, $P = 8 \times 10^{-6}$). Post-hoc comparisons using Dunnett's test showed significant differences from baseline until the second day after lesion (post and 8 h: $P < 0.001$; 1 day: $P = 0.002$; $P > 0.05$ thereafter).

Fig. 3g. Comparisons of HVC dynamics in intact controls and following Nif lesions. A two-tailed, paired t-test revealed significant differences in correlation immediately before and after lesion ($n = 4$ birds; $P = 0.003$). In addition, two-tailed unpaired t-tests showed significant differences between lesion and control conditions at matched time points until the third day post-lesion ($P < 0.03$ before, $P = 0.1$ at the start of the third day).

Fig. 3h. Comparisons of normalized HVC activity in intact controls and following Nif lesion. A two-tailed, paired t-test revealed significant differences in activity immediately before and after lesion ($n = 4$ birds; $P = 0.002$). In addition, two-tailed unpaired t-tests showed significant differences between lesion and control conditions at matched time points until the third day post-lesion ($P < 0.03$ before, $P = 0.29$ at the end of the third day).

Fig. 3i. Top, comparison of recovery of correlation to pre-lesion HVC dynamics during day and night ($n = 4$ birds). Two-tailed one-sample t-tests revealed significant recovery overnight but not during the day (test against mean zero; $P = 0.01$ and $P = 0.053$, respectively). Bottom, comparison of recovery of HVC activity to pre-lesion levels during day and night ($n = 4$ birds). Two-tailed one-sample t-tests revealed significant recovery during the day but not overnight (test against mean zero; $P = 0.007$ and $P = 0.48$, respectively).

Fig. 3j. Top, correlation to pre-lesion HVC dynamics immediately following Nif lesions as a function of the fraction of Nif lesioned ($n = 11$ birds). A two-tailed *t*-test revealed the Pearson's linear correlation coefficient, $R = -0.91$, to be significantly different from zero ($P = 1 \times 10^{-4}$). Bottom, normalized HVC activity immediately following Nif lesions as a function of the fraction of Nif lesioned ($n = 11$ birds). A two-tailed *t*-test revealed the Pearson's linear correlation coefficient, $R = -0.87$, to be significantly different from zero ($P = 5 \times 10^{-4}$).

Fig. 4f. Top, comparison of post-lesion motif completion rates to pre-lesion baseline for unilateral ($n = 4$ birds) and bilateral ($n = 5$ birds) Nif lesions. Repeated measures ANOVA revealed that lesions resulted in significant reductions of completion rates in unilateral ($F_{(8,16)} = 7.0, P = 5 \times 10^{-4}$), but not bilateral ($F_{(6,18)} = 4.1$, $P = 0.07$), lesions. Post-hoc analysis of the unilateral lesion data using Dunnett's test showed motif completion rates to be significantly different from pre-lesion on the day of lesion ($P = 5 \times 10^{-4}$), but not thereafter ($P > 0.11$). Bottom, comparison of post-lesion motif tempo to pre-lesion baseline for birds with unilateral ($n = 4$ birds) and bilateral ($n = 5$ birds) Nif lesions. Repeated measures ANOVA revealed that Nif lesions had a significant effect on motif tempo in both unilateral ($F_{(8,16)} = 10.4$, $P = 4.6 \times 10^{-5}$) and bilateral ($F_{(6,18)} = 17.5$, $P = 1.3 \times 10^{-6}$) conditions. Post-hoc analysis using Dunnett's test showed motif tempo was slowed down for both unilateral and bilateral lesions: the effects remained significant ($P < 0.05$) throughout the 7 days in the bilaterally lesioned birds, and through the first 4 days in unilaterally lesioned birds.

Code availability. All custom-written code will be made available upon request.

51. Poddar, R., Kawai, R. & Ölveczky, B. P. A fully automated high-throughput training system for rodents. *PLoS ONE* **8,** e83171 (2013).
52. Neafsey, E. J. *et al.* The organization of the rat motor cortex: a microstimulation mapping study. *Brain Res.* **396,** 77–96 (1986).
53. Allen, T. A. *et al.* Imaging the spread of reversible brain inactivations using fluorescent muscimol. *J. Neurosci. Methods* **171,** 30–38 (2008).
54. Ölveczky, B. P., Andalman, A. S. & Fee, M. S. Vocal experimentation in the juvenile songbird requires a basal ganglia circuit. *PLoS Biol.* **3,** e153 (2005).
55. Naie, K. & Hahnloser, R. H. R. Regulation of learned vocal behavior by an auditory motor cortical nucleus in juvenile zebra finches. *J. Neurophysiol.* **106,** 291–300 (2011).
56. Ravbar, P., Lipkind, D., Parra, L. C. & Tchernichovski, O. Vocal exploration is locally regulated during song learning. *J. Neurosci.* **32,** 3422–3432 (2012).
57. Tchernichovski, O., Nottebohm, F., Ho, C. E., Pesaran, B. & Mitra, P. P. A procedure for an automated measurement of song similarity. *Anim. Behav.* **59,** 1167–1176 (2000).
58. Fiete, I. R., Senn, W., Wang, C. Z. H. & Hahnloser, R. H. R. Spike-time-dependent plasticity and heterosynaptic competition organize networks to produce long scale-free sequences of neural activity. *Neuron* **65,** 563–576 (2010).

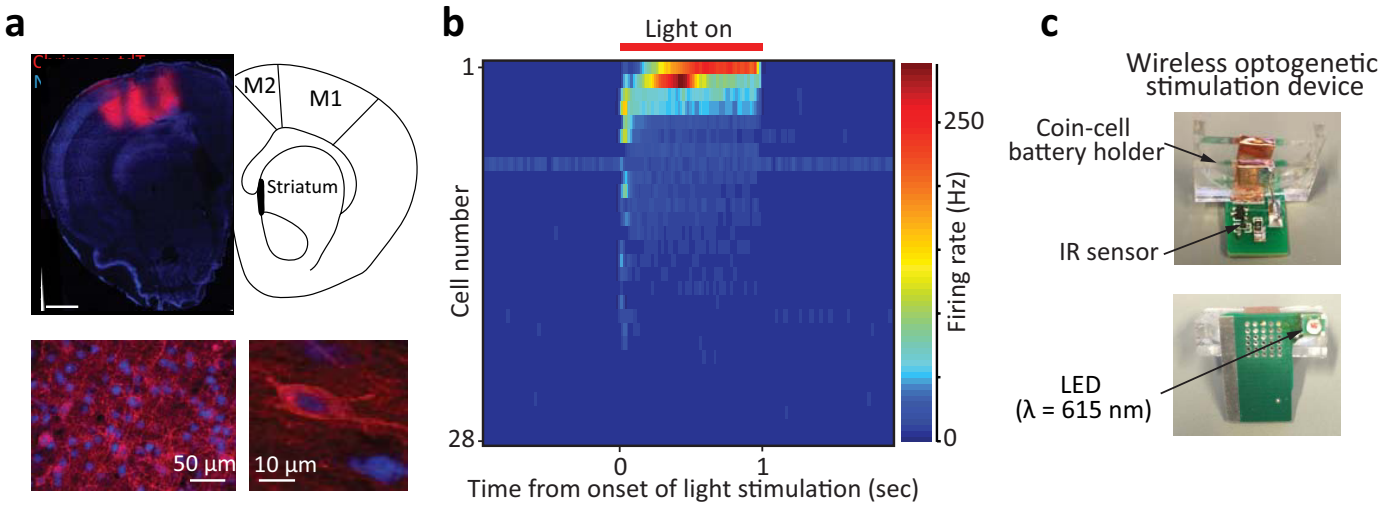

Extended Data Figure 1 | Light stimulation of motor cortical neurons expressing the optogenetic activator Chrimson. a, Representative example of AAV-injections into motor cortex, showing Chrimson-tdTomato expression at different magnifications in a coronal brain section (~1.5 mm anterior to bregma). The scheme of the brain (right) is adapted from Paxinos' rat atlas. The estimated spread of the injections was $8.3 \pm 1.3\ mm^3$ (mean ± s.d., $n = 2$ rats), with an average of 31 ± 2% infected cells (Methods). **b**, Heatmap showing the instantaneous firing rates of 28 single units recorded in an anaesthetized rat in response to a 1 s light pulse, averaged over 30 stimulations (Methods). **c**, A custom-built battery-operated wireless optogenetic stimulation device, consisting of a printed circuit board with integrated IR sensor and LED ($\lambda = 615$ nm). The IR sensor gates the circuit and allows the LED to be triggered by an IR light-source placed on top of the rat's cage. During surgery, the LED is affixed atop a small craniotomy above motor cortex.

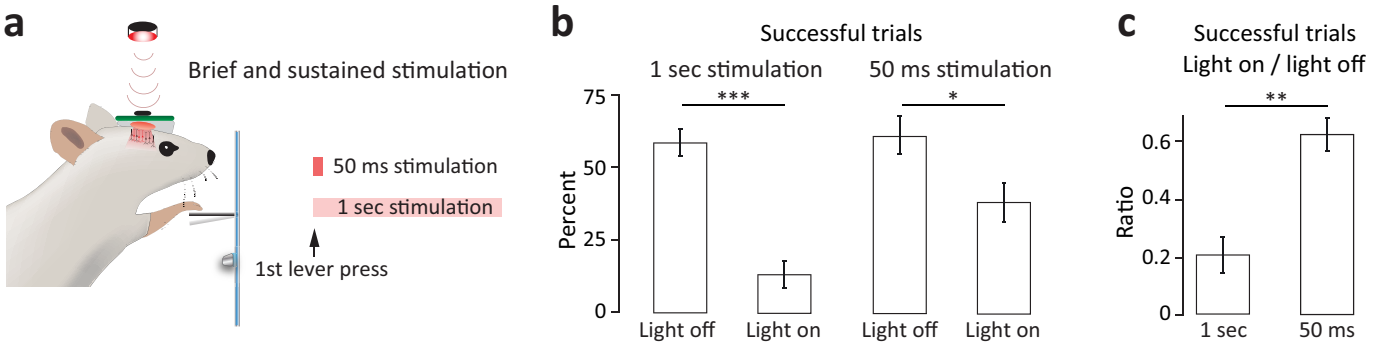

Extended Data Figure 2 | Both brief and sustained optogenetic stimulation of motor cortex cause significant performance deficits in our task. a, Optogenetic stimulation was triggered on the first lever press in a trial, and lasted for either 50 ms or 1 s. **b**, Both sustained (1 s, left, compare Fig. 1h, $n = 5$ rats, $P = 3 \times 10^{-5}$, paired t-test) and brief (50 ms, right, $n = 3$ rats, $P = 0.01$, paired t-test) optogenetic activation of motor cortex interfered with normal task performance. **c**, Comparing the effects of the two stimulation protocols on task performance (ratio light on/light off) shows that sustained stimulation has a significantly larger effect (1 s: $n = 5$; 50 ms: $n = 3$, $P = 0.004$, unpaired t-test). Error bars represent s.e.m.

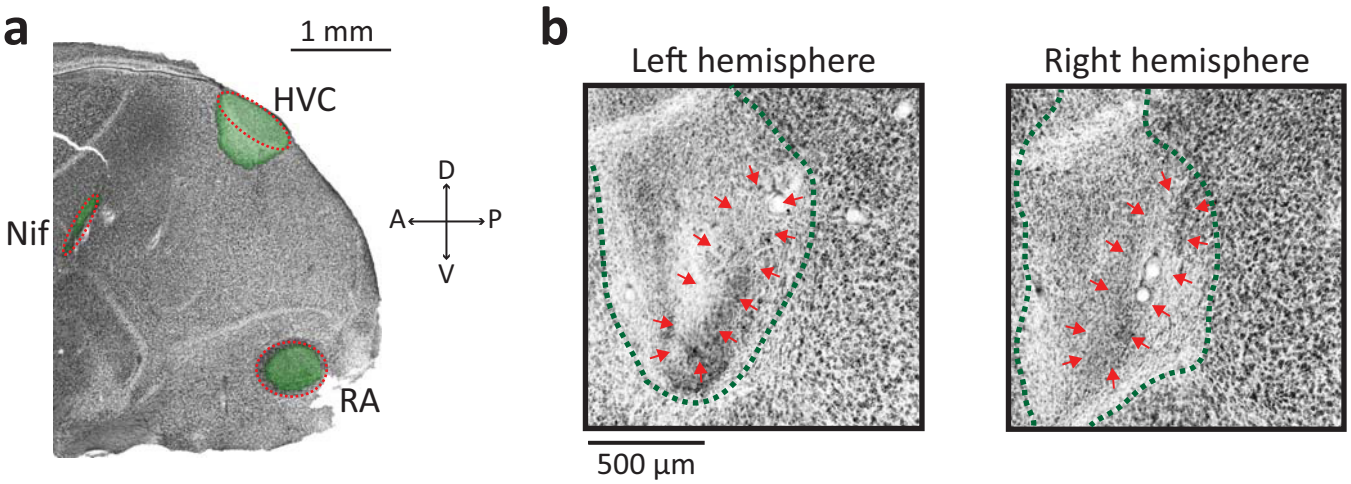

Extended Data Figure 3 | Localization and lesioning of Nif. a, Injection of fluorescently labelled cholera toxin subunit B (green) into HVC retrogradely labels Nif and anterogradely labels downstream control nucleus RA. **b**, Bilateral injections of the excitotoxin NMA produced focal lesions of Nif. Shown are Nissl stained sections from both hemispheres in the same example bird. Red arrows indicate the estimated boundaries of Nif; dashed green line shows the extent of the lesion.

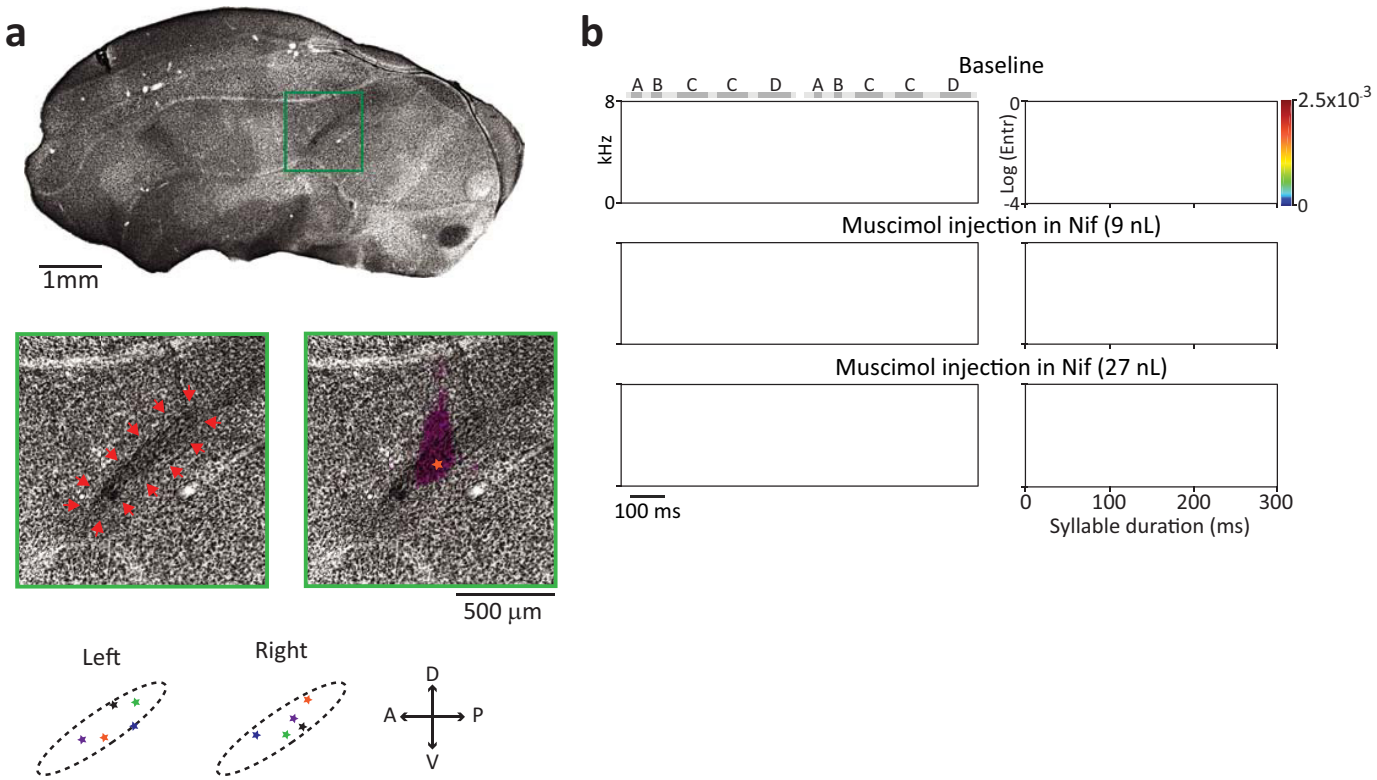

Extended Data Figure 4 | Muscimol injections into Nif. a, Top, Nissl-stained parasagittal section of a zebra finch brain. Middle, magnified view of the region demarcated with a green square atop. Red arrows (left) indicate the estimated boundaries of Nif; violet overlay (right) shows the spread of fluorescent dye co-injected with muscimol. Orange star indicates estimated centre of injection based on brightness of the fluorescence. Bottom, estimated injection sites relative to the boundaries of Nif for all muscimol-injected birds. Colours denote different animals. **b**, Syllable spectrograms (left) and entropy-duration distributions (right) for a bird injected with different volumes of muscimol in Nif. Example spectrograms for 9 nl and 27 nl injections are from recordings made 3 min and 7 min after the injections, respectively. That song disruption was similarly rapid and severe for both volumes (in conjunction with the lack of effect from injections above Nif) limits the possibility that the effects on song were due to diffusion of the drug into HVC.

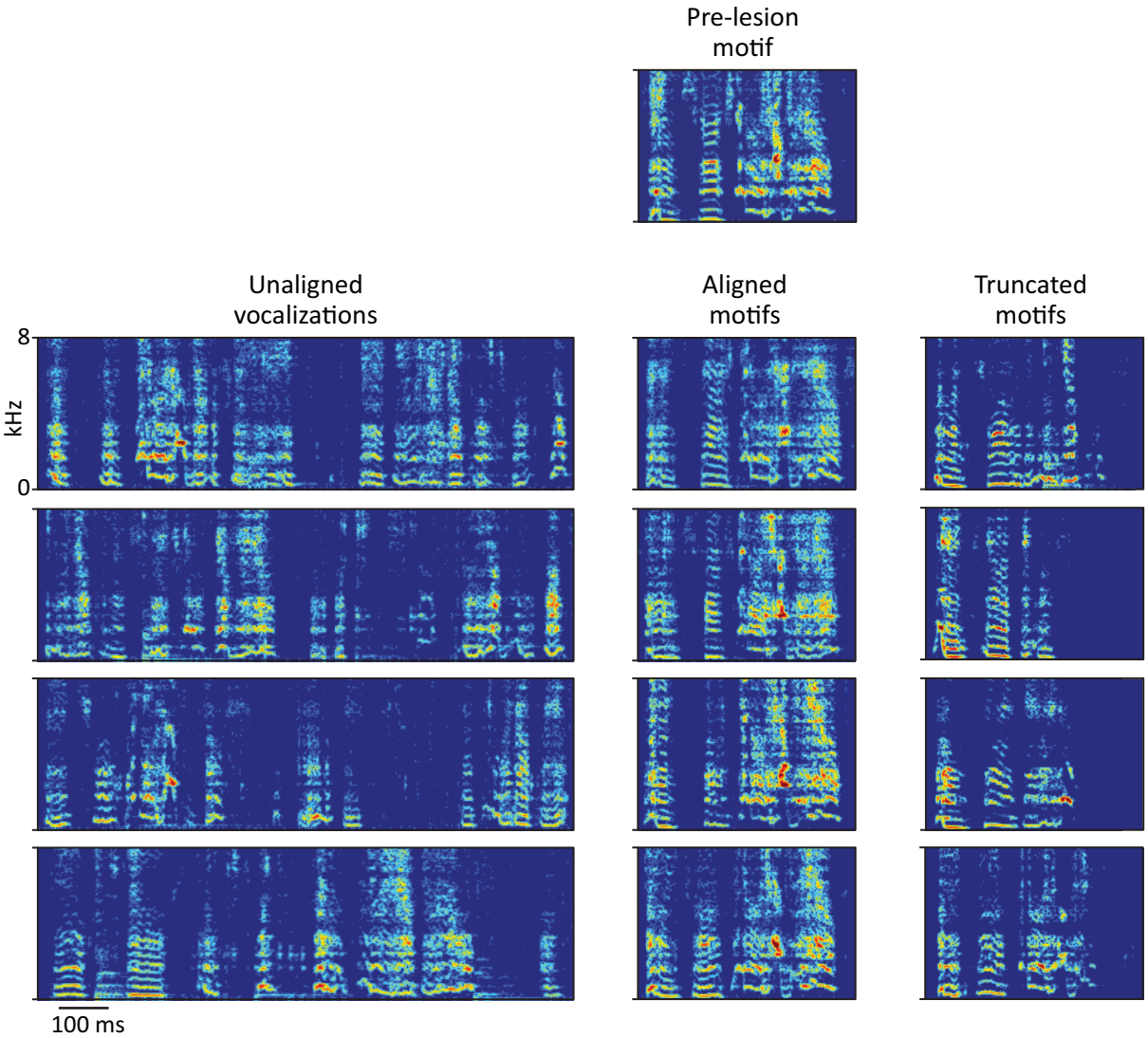

Extended Data Figure 5 | Spectrograms of vocalizations following unilateral Nif lesion. Data for the example bird in Fig. 3. All examples were recorded within the first hour of singing after lesion. Top, example spectrogram of a motif recorded just before lesion. Left, example spectrograms of vocalizations in which motif syllables could not be reliably identified and thus were excluded from subsequent analysis. Middle, example spectrograms of identifiable motifs that were included in the alignment-dependent analysis (Fig. 3f–j). Right, example spectrograms of songs with identifiable syllables, but truncated motifs.

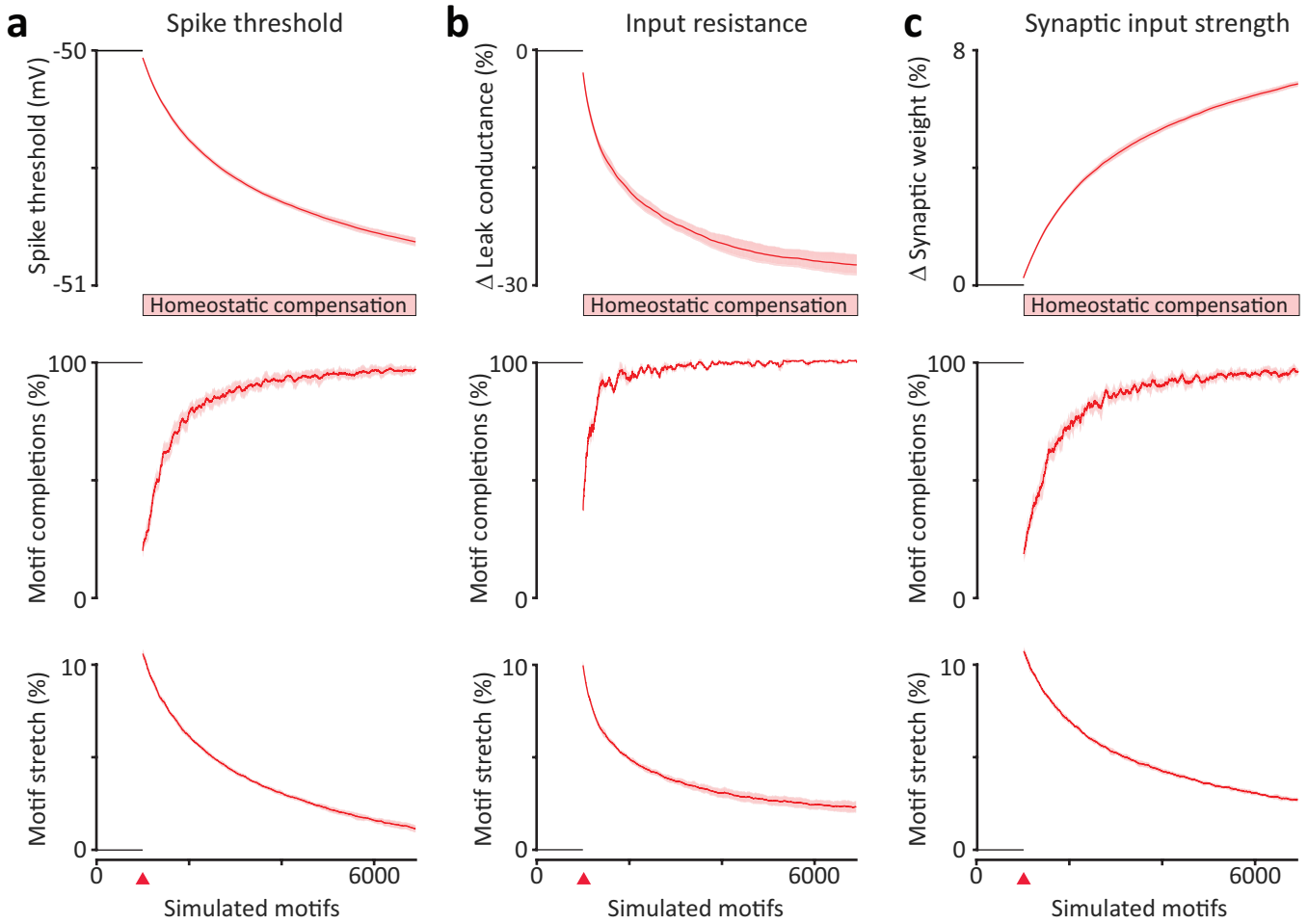

Extended Data Figure 6 | Different mechanisms for homeostatic regulation of neural activity produce similar effects. a, Top, effect of Nif removal on membrane excitability during simulated songs in a model neuron (from the 40th node), smoothed with a 100-point moving average and averaged over 40 model 'experiments' (shaded regions denote standard deviation across 'experiments'). A rule for homeostatic regulation of activity drives a reduction in spiking threshold after Nif removal. Middle, fraction of simulations in a 100-point window for which activity in the model HVC network propagated to the end, averaged over 40 model 'experiments' (Methods). Bottom, a 100-point moving average over the time to complete a full chain propagation, averaged over 40 model 'experiments'. Orange triangle denotes time of Nif removal. Same as in Fig. 4b, d. **b**, **c**, Same as in **a**, but with homeostatic regulation of membrane leak conductance (**b**) and synaptic input strength (**c**) (Methods).